S. Soldini, C. Colombo, S. Walker
The End-Of-life Disposal of Satellites in Libration-Point Orbits Using Solar Radiation Pressure
Advances in Space Research, Vol. 57, N. 8, 2016, p. 1664-1679
doi:10.1016/j.asr.2015.06.033

The end-of-life disposal of satellites in Libration-point orbits using solar radiation pressure

Stefania Soldini [1]

Astronautics Research Group, University of Southampton, Southampton, SO171BJ, United Kingdom

Camilla Colombo [2] Scott Walker [3]

Astronautics Research Group, University of Southampton, Southampton, SO171BJ, United Kingdom

Abstract

This paper proposes an end-of-life propellant-free disposal strategy for Libration-point orbits which uses solar radiation pressure to restrict the evolution of the spacecraft motion. The spacecraft is initially disposed into the unstable manifold leaving the Libration-point orbit, before a reflective sun-pointing surface is deployed to enhance the effect of solar radiation pressure. Therefore, the consequent increase in energy prevents the spacecraft's return to Earth. Three European Space Agency missions are selected as test case scenarios: Herschel, SOHO and Gaia. Guidelines for the end-of-life disposal of future Libration-point orbit missions are proposed and a preliminary study on the effect of the Earth's orbital eccentricity on the disposal strategy is shown for the Gaia mission.

Keywords: End-of-life disposal; Solar radiation pressure; Circular restricted-three body problem; Elliptic restricted-three body problem; Zero-velocity curves

[1]Corresponding author: PhD candidate, s.soldini@soton.ac.uk
[2]Lecturer, currently Marie Curie Research Fellow, c.colombo@soton.ac.uk
[3]Associate Professor, sjiw@soton.ac.uk

Acronyms

AU Astronomical Unit

CR3BP Circular Restricted Three Body Problem

EOL End-Of-Life

ER3BP Elliptic Restricted Three Body Problem

ESA European Space Agency

GEO Geosynchronous Equatorial Orbit

JAXA Japan Aerospace Exploration Agency

LPO Libration-Point Orbit

SRP Solar Radiation Pressure

ZVC Zero Velocity Curve

Nomenclature

L_j/SL_j	j^{th} collinear Lagrangian/Pseudo-Lagrangian point with $j = 1, \ldots, 3$
U	Total potenianl energy which includes the rotating system potential and the gravitational potential
U_s	Potential of SRP
$_x$, $_y$ and $_z$	Derivatives with respect to x, y and z
r_{Sun-p} and $r_{Earth-p}$	Spacecraft (p) and Sun and Earth distances respectively
m_{Earth}	Earth's mass [kg]
M_{Sun}	Sun's mass [kg]
μ	Mass parameter ($m_{Earth}/(M_{Sun} + m_{Earth})$) for the Sun-(Earth+Moon) system is equal to $3.04042 \cdot 10^{-6}$
x_{Sun} and x_{Earth}	Sun ($-\mu$) and Earth ($1 - \mu$) positions respectively
μ_{Sun} and μ_{Earth}	Sun ($1 - \mu$) and Earth (μ) unit masses respectively
m	Spacecraft's mass [kg]
A	Spaceraft's reflective area [m^2]

σ	Mass-to-area ratio (m/A) [kg m^{-2}]
σ^*	Sun luminosity, 1.53 [g m^{-2}]
β	Lightness parameter (σ^*/σ)
c_R	Reflective coefficient
$P_{srp-1AU}$	Sun pressure at 1AU
$r_{Earth-Sun}$	Earth to Sun distance
x_{SL_j}	Position of the collinear Pseudo-Lagrangian point
E	Energy of the system
β_0	Lightness paramiter for the spacecraft's initial dry area-to-mass ratio
Δv	Variation in the spacecraft's velocity after a manoeuvre
ΔE	Variation of energy between the spacecraft and L_j or SL_j
E_{SL_j}	Energy of the Pseudo-Lagrangian point
$\Delta\beta$	Contribution of the increased area of the spacecraft after the deployment where $\beta = \beta_0 + \Delta\beta$
V	Magnitude of the spacecraft's velocity
V_{clsr}	Spacecraft's velocity required after the Δv manoeuvre
Δv_{eq}	Theoretical Δv
R	Correspond to 60,000 [km]
$d_{Earth-p}$	Spacecraft-Earth distance
$\boldsymbol{r}_{Earth}$ and $\boldsymbol{r}_p$	Distances of the Earth and the spacecraft from the center of mass
A_0	Initial spacecraft's deployable area [m^2]
m_{dry}	Dry mass [kg]
A_0/m_{dry}	Initial area-to-mass ratio [m^2 kg^{-1}]
r	Earth+Moon distance from the Sun [km]
a	Semimajor axis [km]
f	True anomaly [rad]
e	Earth's orbit eccentricity
$\dot{f}$	Angular velocity [rad s^{-1}]
h	Angular momentum [km^2 s^{-1}]
$M_{Earth+Moon}$	Earth+Moon mass [kg]
G	Costant of gravitation [N m^2 kg^{-2}]
$\tilde{\mu}$	$G \cdot (M_{Sun} + M_{Earth+Moon})$ [km^3 s^{-2}]
ω, Ω and Ω'	Potential energy in the ER3BP

$\boldsymbol{r}_d$ and $\dot{\boldsymbol{r}}_d$	Dimentional position [km] and velocity [km s^{-1}] coordinates
$\boldsymbol{r}$ and $\boldsymbol{r}'$	Non-dimentional pulsating position and velocity coordinates
I	Energy integral
f_0	Initial true anomaly when leaving the LPO [rad]

1. Introduction

Libration-Point Orbit (LPO) missions are often selected for studying the Sun and the Universe. Orbits around the Libration points L_1 and L_2 of the Sun-Earth system are advantageous as they can be reached from the Earth and, since a constant sky field of view is ensured with respect to the Sun and the Earth, they are frequently used for space observation. There are also further advantages regarding the ease of Earth communication and in the thermal system design. However, they lie in highly perturbed regions; therefore, an uncontrolled spacecraft would naturally follow the unstable manifold and after several years could cross the protected regions at the Earth and the L_1/L_2 regions. In addition, since LPO spacecraft are characterised by large dry masses, it is critical to clear these regions once the mission has ended.

Possible disposal strategies for LPO missions were investigated as a result of a European Space Agency (ESA) study on End-Of-Life (EOL) disposal concepts for Lagrange-Point and Highly Elliptical Orbit Missions. The natural multi-body dynamics in the Earth environment and in the Sun-Earth system were exploited. The main idea is to either restrict the motion of the spacecraft to specific regions or to destroy the spacecraft through an impact with another body. The options investigated were Earth's re-entry, injection onto trajectories towards a Moon impact, heliocentric parking orbit by means of Δv or heliocentric parking orbit by means of Solar Radiation Pressure (SRP) (Colombo et al., 2015, 2014).

Olikara et al. (2013) initially proposed a disposal option, which injects the spacecraft towards the inner or the outer solar system and closes the Hill's surfaces though a Δv manoeuvre at L_1 or L_2. Olikara et al. (2013) suggested that the overall return trajectories to the Earth in the Circular Restricted Three Body Problem (CR3BP) and in the full-body (ephemerides) are quite similar.

In this article, an alternative disposal strategy is investigated that allows the closure of the zero-velocity curves by means of SRP. In this case, the spacecraft is disposed at the EOL onto the unstable manifold leaving the LPO from L_2. An energetic approach is used to close the Hill's curves at SL_2 (*e.g.*, the pseudo Libration-point L_2 when SRP is added (McInnes, 2000)) by increasing the energy of the system and then computing the reflective deployable area required for the EOL curves-closure. As a term due to SRP is added to the energy, the shape of the potential surfaces changes and the required reflective area is computed via numerical optimisation, imposing the condition for the curves closure at SL_2. After the closure, the spacecraft is bounded in its following motion at the right-hand side of the pseudo Libration point, thus, preventing the spacecraft's return to the Earth and protecting the L_2 region. It is also demonstrated that the spacecraft cannot be confined towards the inner solar system due to the constraint in the direction of SRP acceleration and that the disposal through SRP can only be performed at SL_2. This strategy can be achieved through a sun-pointing auto-stabilised deployable structure, such as light reflective surfaces that are already proven for attitude control applications (*e.g.*, GOES's cone solar sail [4] (DRL-101-08, 1996)), with the advantage of saving propellant.

Three ESA missions are selected as scenarios: Herschel (Bauske, 2009), which investigates the formation of galaxies, SOHO (Olive et al., 2013), which studies the Sun's outer corona and the solar wind and Gaia (Hechler and Cobos, 2002), a space telescope. Results show that the area required is lower if the deployment is performed further away from the Sun. Moreover, higher initial energy requires a larger deployed area at a fixed distance from the Sun. For robustness, the effect of the Earth's orbit eccentricity for the Gaia mission is also investigated in order to include a safety margin into the deployed area. Indeed, Campagnola et al. (2008) demonstrated that small perturbations in the CR3BP due to the Earth's orbit eccentricity affect the closure of the zero-velocity curves and Hyeraci and Topputo (2013) investigated the same effect in the ballistic capture trajectories.

Instead, this paper investigates how the effect of the true anomaly affects the EOL disposal enhanced by SRP. It is required to model the Elliptic Restricted Three Body dynamics with the effect of SRP (ER3BP-SRP) (Szebehely and Giacaglia, 1964; Baoyin and McInnes, 2006), to derive the

[4] The cone shape of the sail guarantees attitude passive stabilisation.

transformation from a synodic frame in dimensional coordinates to the sidereal frame in non-dimensional and pulsating coordinates and to define the energy in the synodic system. Results demonstrate that a deployable area margin is needed when including the eccentricity effect.

Finally, guidelines for EOL disposal of future LPO missions are proposed. The aim of this study is to find the reflective area required for the disposal and to investigate if it is necessary to use specifically designed deployable reflective areas, or if it is possible to exploit some existing reflective deployable areas and then, at the EOL, change their original configuration to achieve the zero-velocity curves closure. Through this strategy, any existing area deployable structures on-board the spacecraft can be exploited by deploying an additional area such as solar panel flaps or a modified sunshield geometry.

2. Circular restricted-three body problem with the effect of solar radiation pressure

The spacecraft's motion is approximated in the Circular Restricted Three-Body Problem (CR3BP) and the effect of the SRP is included into the dynamics at the moment of the zero-velocity curves closure in SL_2. Therefore, in this section, the CR3BP dynamics with SRP (CR3BP-SRP) will be presented (McInnes, 2000). The dynamics are written in the non-dimensional rotating coordinate frame (synodic system) (Szebehely, 1967) as:

$$\begin{cases} \ddot{x} - 2\dot{y} = -U_x(x,y,z) - U_{s_x}(x,y,z,\beta) \\ \ddot{y} + 2\dot{x} = -U_y(x,y,z) - U_{s_y}(x,y,z,\beta) \\ \ddot{z} = -U_z(x,y,z) - U_{s_z}(x,y,z,\beta) \end{cases} \tag{1}$$

where, $U(x,y,z)$ is the total potential which includes the contribution of the rotating system potential and the gravitational potential,

$$U(x,y,z) = -\frac{1}{2}(x^2+y^2) - \frac{\mu_{Sun}}{r_{Sun-p}} - \frac{\mu_{Earth}}{r_{Earth-p}}. \tag{2}$$

In Eq. (2), r_{Sun-p} and $r_{Earth-p}$ are, respectively, the spacecraft's (p) distance from the Sun and the Earth:

$$r_{Sun-p} = \sqrt{(x - x_{Sun})^2 + y^2 + z^2} \tag{3}$$

and

$$r_{Earth-p} = \sqrt{(x - x_{Earth})^2 + y^2 + z^2}. \tag{4}$$

In non-dimensional coordinates, $x_{Sun} = -\mu$ is the position of the Sun and $x_{Earth} = 1 - \mu$ is the position of the Earth+Moon barycentre. The primaries unit masses are defined as $\mu_{Earth} = \mu$ and $\mu_{Sun} = 1 - \mu$ where, $\mu = \frac{m_{Earth}}{M_{Sun}+m_{Earth}}$ is the mass parameter of the Sun-(Earth+Moon) system, equal to $3.04042 \cdot 10^{-6}$. In non-dimensional coordinates, the angular velocity of the synodic system at the barycentre is the mean motion and it is equal to 1.

The SRP model used in this study is the cannonball model, which gives a first approximation of the solar radiation effect when included in the CR3BP-SRP or ER3BP-SRP dynamics. For a Sun-pointing reflective surface, the potential of the SRP force is:

$$U_s = \beta \frac{\mu_{Sun}}{r_{Sun-p}}. \tag{5}$$

In Eq. (5), $\beta = \frac{\sigma^*}{\sigma}$ is the lightness parameter and it is a function of the area-to-mass ratio and the Sun luminosity as $\sigma = \frac{m}{A}$ and $\sigma^* = \frac{L_{Sun}}{2\pi c \mu_{Sun}} = 1.53$ [g/m^2] (McInnes, 1998) for the specific case, where the reflectivity coefficient (c_R) is 2. Moreover, β is defined within the range of 0 (no SRP effect) and 1 (SRP counteracts the gravitational effect of the Sun). From Eq. (5) the acceleration due to SRP can be derived as $-\nabla U_s \hat{\boldsymbol{r}}$ to give:

$$\boldsymbol{a}_{srp} = \beta \frac{\mu_{Sun}}{r^2_{Sun-p}} \hat{\boldsymbol{r}}. \tag{6}$$

However, for a non near-perfect reflective structure, it is convenient to write β as a function of c_R:

$$\boldsymbol{a}_{srp} = P_{srp-1AU} \left(\frac{r_{Earth-Sun}}{r_{Sun-p}} \right)^2 \frac{A}{m} c_R \hat{\boldsymbol{r}}, \tag{7}$$

where $P_{srp-1AU}$ is the Sun pressure at 1 AU and $r_{Earth-Sun}$ is the Earth to Sun distance. To express β as a function of c_R, we now equal Eq. (6) with Eq. (7) and the lightness parameter is then defined as:

$$\beta = P_{srp-1AU} \frac{r^2_{Earth-Sun}}{\mu_{Sun}} \frac{A}{m} c_R. \tag{8}$$

2.1. Collinear Lagrangian points with SRP

When adding SRP, it is possible to find a new equilibrium solution for the CR3BP-SRP. This modified equations of motion results in surfaces of

"artificial" libration points as a function of the sail orientation angle, so now the system has a 2D family of equilibrium points (McInnes, 2000; Farrés and Jorba, 2010). The equilibrium points are the zero velocity points in the rotating frame which correspond to singular solutions on the equipotential surface. These points corresponds to the positions in the rotating frame in which the gravitational forces, SRP forces and the centrifugal forces are cancelled out. At these particular positions, a spacecraft appears stationary in the synodic frame. For the collinear solutions $y = 0$, this means that the equilibrium points, that lie on the x-axis, exist if only the surface is sun-pointing, and by setting to zero the velocities and the accelerations of Eq. (1), the equations turn into:

$$\begin{cases} -U_x(x,y,z) - U_{s_x}(x,y,z,\beta) = x - \frac{(1-\beta)\mu_{Sun}(x-x_{Sun})}{r^3_{Sun-p}} - \frac{\mu_{Earth}(x-x_{Earth})}{r^3_{Earth-p}} = 0 \\ -U_y(x,y,z) - U_{s_y}(x,y,z,\beta) = y - \frac{(1-\beta)\mu_{Sun}}{r^3_{Sun-p}}y - \frac{\mu_{Earth}}{r^3_{Earth-p}}y = 0 \\ -U_z(x,y,z) - U_{s_z}(x,y,z,\beta) = -\frac{(1-\beta)\mu_{Sun}}{r^3_{Sun-p}}z - \frac{\mu_{Earth}}{r^3_{Earth-p}}z = 0. \end{cases} \tag{9}$$

The position along the x-axis can be finally computed by solving Eq. (10):

$$x_{SL_j} - \frac{(1-\beta)\mu_{Sun}(x_{SL_j} - x_{Sun})}{r^3_{Sun-p}} - \frac{\mu_{Earth}(x_{SL_j} - x_{Earth})}{r^3_{Earth-p}} = 0. \tag{10}$$

The fifth-order polynomial coefficients depend on the space region in which the equilibrium points abscissa is defined. The range of validity for the collinear Lagrangian points are:

$$\begin{cases} -\mu \leq x_{SL_1} \leq 1-\mu \\ -\mu \leq 1-\mu \leq x_{SL_2} \\ x_{SL_3} \leq -\mu \leq 1-\mu \end{cases} . \tag{11}$$

The fifth-order polynomials in Table 1 have five roots in which one is real and the other four are complex, Elipe (1992) presented these coefficients for a binary-star system[5]. The positions of the collinear points on the x-axis correspond to the real root.

Figure 1 shows the position of the collinear points as a function of β for a Sun pointing surface, where μ is set to the one for the Sun-(Earth+Moon)

[5]Please note that there is a typo in the coefficients of Eq. 14 in Ref. (Elipe, 1992), when only one of the stars is considered.

system. The case of $\beta = 0$ represents the CR3BP without solar radiation pressure; on the other hand, when $\beta = 1$ the CR3BP-SRP dynamics degenerates into the two body problem dynamics in a rotating frame. When β tends to 1 the SRP counteracts completely the gravitational effect of the Sun, SL_1 and SL_3 converge to the origin of the system (which is the center of mass). This mean that by increasing β the positions of SL_1 and SL_3 move closer to the Sun, and the position of SL_2 gets closer to the Earth, due to the balancing of the gravitational acceleration, the Coriolis acceleration, and the solar radiation pressure accelerations. Finally, the trend of this graph is also sensitive to the value of μ.

Table 1: Fifth-order polynomial coefficients for determining the Lagrangian points with SRP.

SL_j	x^5	x^4	x^3	x^2	x	*Constant*
SL_1	1	$-(3-\mu)$	$(3-2\mu)$	$-(\mu+\beta\mu_{Sun})$	2μ	$-\mu$
SL_2	1	$(3-\mu)$	$(3-2\mu)$	$-(\mu-\beta\mu_{Sun})$	-2μ	$-\mu$
SL_3	1	$(2+\mu)$	$(1+2\mu)$	$-(1-\beta)\mu_{Sun}$	$-2(1-\beta)\mu_{Sun}$	$-(1-\beta)\mu_{Sun}$

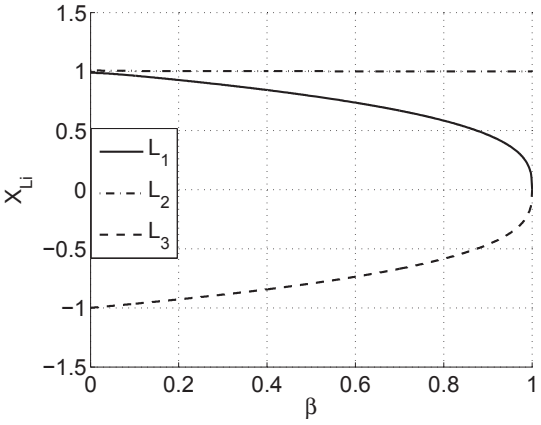

Figure 1: Collinear Lagrangian points for $\beta \neq 0$ and $\mu = 3.036 \cdot 10^{-6}$.

2.2. Energy, zero-velocity curves and forbidden region

The energy with the effect of solar radiation pressure is defined as:

$$E(x, y, z, \dot{x}, \dot{y}, \dot{z}, \beta_0) = \frac{1}{2}(\dot{x}^2 + \dot{y}^2 + \dot{z}^2) + U(x, y, z) + U_s(x, y, z, \beta_0) \quad (12)$$

where, β_0 is given by the effect of the spacecraft's initial dry area-to-mass ratio [6] and $U(x, y, z)$ is defined as in Eq. (2). The zero-velocity curves for a Sun-pointing area are given by the intersection of the energy of the spacecraft with the total potential in Eq. (2) plus the contribution of SRP given by Eq. (5). The aim here is to close the zero-velocity curves at the pseudo Libration point, SL_2, in order to safely dispose of the spacecraft into a graveyard orbit around the Sun. In the strategy presented by Olikara et al. (2013), after a Δv manoeuvre to close the zero-velocity curves, it is necessary to verify that the motion of the spacecraft is still permitted. Thus, a check on to the forbidden region is required when using traditional propulsion. Instead, in case of SRP manoeuvre, the velocity of the spacecraft before and after the deployment doesn't change. For this reason if a value in β is found that closes the zero-velocity curves, then this ensures that the motion of the spacecraft is still permitted after the deployment. Indeed the Δ energy required to close the zero velocity curves depends just on the effect of SRP:

$$\Delta E = E_{SL_2} - E = U_s, \quad (13)$$

where E_{SL_2} is the energy of SL_2, E is the energy of the spacecraft before the deployment in Eq. (12) and U_s is defined as Eq. (5) by setting $\beta = \Delta\beta$.

3. End-of-life disposal through solar radiation pressure

For the EOL disposal enhanced by SRP, the main goal is to find the minimum deployable area required to close the zero-velocity curves at the pseudo libration point, SL_2, in order to confine the motion of the spacecraft outside the Earth-L_2 protected regions. The minimum area is determined through numerical optimisation by satisfying the constraint that the additional area should increase the energy of the system in order to reach the energy at the pseudo libration point.

[6] At the EOL, the area-to-mass ratio is close to the dry area-to-mass ratio since the fuel almost runs out when the mission ends.

To design a strategy that enables the solar radiation pressure to be used to close the zero velocity curves at SL_2, we need to compute the unstable manifold towards the outer part of the system. The unstable manifold is computed by integrating the trajectory forward in time with a perturbation of $+\epsilon = 10^{-6}$ which corresponds to a displacement error in the spacecraft position of $D = 200$ km (Koon et al., 2008; Goméz et al., 1991a).

Figure 2 shows an example of the SRP disposal strategy for a two dimensional case. The time used for the manifold evolution is about 400 non-dimensional time units; which corresponds to 63.5 years. A number of trajectories (in grey, Figure 2a) which belong to this unstable tube are selected with their initial condition close to the LPO. As can be seen from Figure 2a, the disposal strategy to inject the spacecraft towards the unstable manifolds without closing the zero velocity curves is unsafe. Indeed, the disposed spacecraft could represent a potential hazard to other operating spacecraft in LPOs or to the Earth; hence this approach is not sustainable. In particular, the highlighted trajectory in Figure 2a (bold black line) shows that after 29.5 years the spacecraft will encounter the Earth and the L_2 regions since the zero-velocity curves have a trajectory gateway at L_2. A point P_1 along each natural trajectory legs is selected (Figure 2b), where a sun-pointing reflective surface is deployed (Figure 2c). This allows the closure of the zero velocity curves at SL_2. The trajectories evolution after the deployment of the SRP enhancing device was verified by computing the new trajectory legs with the added effect of β (Figure 2d). In this case, β corresponds to a value of 0.00132[7]. It can be verified that, in correspondence of any point of the following evolution, the zero velocities curves are closed (see dashed line in Figure 2d). By enhancing the effect of SRP, the energy of the system was changed without any propellant costs. Afterwards, the energy does not change along the resulting trajectory if the deployable area is passively stabilised with the Sun. Finally, even if the L_2-LPO region is not completely protected (Figure 2d), the probability of crossing region close to L_2 is now lower. It is interesting to note that, with respect to the strategy proposed by Olikara et al. (2013), here the energy is increased rather than decreased as it will be demonstrated later.

[7]This value of β corresponds to 861 m^2 for a 1000 kg of spacecraft.

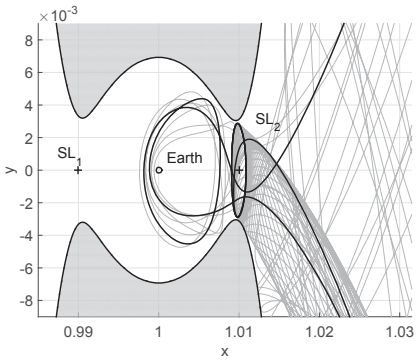

(a) Unstable manifold: the highlighted trajectory encounters the Earth after 29.5 years.

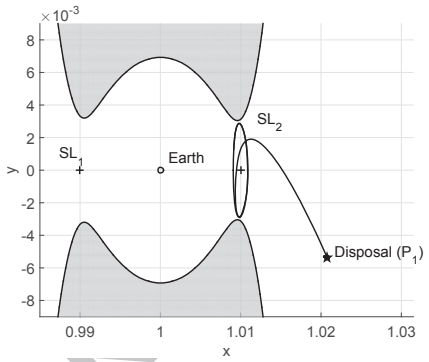

(b) Selected trajectory where the deployment is done after 68.04 days from the leaving LPO.

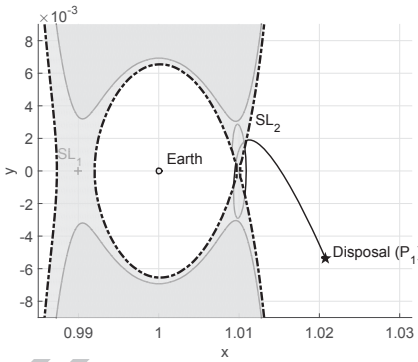

(c) Deployment of a Sun-pointing area in P_1 to close the zero-velocity curves in SL_2

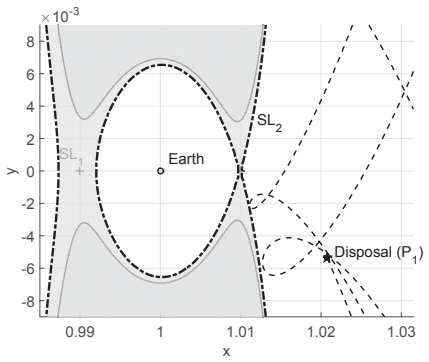

(d) Trajectory evolution after the deployment in P_1, black dashed is integrated for 63.5 years.

Figure 2: End-of-life disposal manoeuvre at 68.04 days since the manifold injection, with 63.5 years of trajectory evolution. This is a critical case to make the strategy more clear, i.e. before the deployment the SRP was zero.

4. Energy approach in the CR3BP-SRP

The spacecraft is supposed to be equipped with a deployable EOL device, to close the zero velocity curves at SL_2. This device is configured to be Sun-pointing and auto-stabilised, so the SRP force admits a potential form (DRL-101-08, 1996; Ceriotti et al., 2014). The same formulation was analysed in two different cases: the first one when the effect of SRP is taken into account only after the surface deployment and the second one when the effect of SRP is considered since the injection into the manifold and then the minimum area required is computed as a delta SRP effect due to, for example, the deployment of reflective flaps from the original spacecraft sunshade configuration. In this paper, only the second case is discussed because including the SRP from the manifold injection influences the manifold evolutions (i.e., small perturbations in the position), while the required reflective area for the disposal is very similar in the two cases. When a near-perfect reflective flap is deployed, the energy increases to:

$$E(x,y,z,\dot{x},\dot{y},\dot{z},\beta_0,\Delta\beta) = \frac{1}{2}(\dot{x}^2+\dot{y}^2+\dot{z}^2) + U(x,y,z) + U_s(x,y,z,\beta_0+\Delta\beta) \tag{14}$$

where, β_0 represents the nominal spacecraft configuration and $\Delta\beta$ the effect of the additional area. By expressing all the terms in Eq. (14), it can be rewritten as:

$$E(\boldsymbol{x},\beta_0,\Delta\beta) = \frac{1}{2}V^2 - \frac{1}{2}(x^2+y^2) - (1-\beta_0)\frac{\mu_{Sun}}{r_{Sun-p}} - \frac{\mu_{Earth}}{r_{Earth-p}} + \Delta\beta\frac{\mu_{Sun}}{r_{Sun-p}} \tag{15}$$

where, V is the magnitude of the spacecraft velocity $\{\dot{x},\dot{y},\dot{z}\}$ along the manifolds (before the deployment $\beta=\beta_0$, in Eq. (1)). In order to find the minimum area required to close the zero velocity curves at SL_1 or SL_2, it is necessary to satisfy the following constraint:

$$E(\boldsymbol{x}_{SL_j},\beta_0,\Delta\beta_{min}) = E(\boldsymbol{x}_{P_1},\beta_0,\Delta\beta_{min}) \tag{16}$$

where, $\boldsymbol{x}_{SL_j} = \left\{x_{SL_j},0,0,0,0,0\right\}$ is the position of the collinear Lagrange point with SRP. So Eq. (16) can be written as:

$$\begin{aligned}\tfrac{1}{2}V_{P_1}^2 = \;& \tfrac{1}{2}(x_{P_1}^2+y_{P_1}^2-x_{SL_j}^2) - \mu_{Sun}(1-\beta_0)\left[\frac{1}{r_{Sun-SL_j}}-\frac{1}{r_{Sun-P_1}}\right] \\ & -\mu_{Earth}\left[\frac{1}{r_{Earth-SL_j}}-\frac{1}{r_{Earth-P_1}}\right] + \mu_{Sun}\Delta\beta\left[\frac{1}{r_{Sun-SL_j}}-\frac{1}{r_{Sun-P_1}}\right]\end{aligned} \tag{17}$$

where the index "j" refers to the location (either SL_1 or SL_2) where the closure occurs. From the numerical point of view the boundaries of $\Delta\beta$ required during the optimisation are 0 and 1-β_0. Note that the expression of $\Delta\beta$ cannot be found explicitly from Eq. (17) since the position of the pseudo libration point is function of $\Delta\beta$ as well, see Table 1, thus a numerical optimisation is required. If we compare this strategy with the strategy by Olikara et al. (2013), where a Δv manoeuvre is used to close the curves, the energy is here increased, as in Figure 3b (dashed line), rather than decreased (dashed line in Figure 3a), since the shape of the potential also changes as a result of the effect of SRP (light gray line in Figure 3b). Figure 3 is done for a value of $\mu = 0.3$ to aid visualisation, where in both cases the black straight line corresponds to the energy of the spacecraft before the disposal.

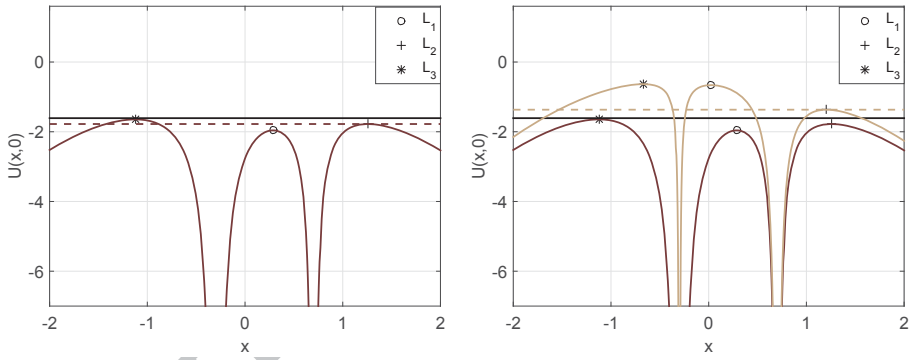

(a) Due to a traditional Δv manoeuvre, the energy of the system decreases to reach the energy of L_2 (dashed line).

(b) Due to the effect of a deployable area, the energy of the system increases to reach the energy of SL_2 (dashed line).

Figure 3: Comparison between the traditional Δv and SRP disposal strategies.

We will now investigate the constraints in the SRP strategy with respect to the traditional Δv. When using SRP, β can assume a value between 0 and 1 thus limiting the value assumed by the energy at the pseudo libration point, SL_j. Moreover, the acceleration of SRP is constrained in direction and this will limit the location of the spacecraft's motion after the deployment.

To demonstrate this, without loss of generality, we simplify the problem to a planar motion with $\beta_0 = 0$, therefore $\beta = \beta_0 + \Delta\beta = \Delta\beta$. For simplicity

a state vector P_1 that has only one non zero component in the x-direction and a velocity magnitude which respects the conservation of the energy is considered here. It is possible to investigate when the energy intersection, in Eq. (16) is feasible for the zero velocity closure in SL_j. Figure 4 and Figure 5 displays the right (i.e., coloured gray scale line) and the left (i.e., black line) side of Eq. (16) evaluated at SL_1 and SL_2, respectively for different values of β. As it can be seen, a feasible solution does not always exist that allows the Hill's curves to be closed. This is evident in Figure 4 for the solution $x = 0.65$. As already mentioned, β is constrained within 0 and 1, so the value of the increased energy is constrained (see Table 2). Finally, it is interesting to note that, by comparing Figure 4 and Figure 5, a lower β is required to close the zero velocity curves in SL_2.

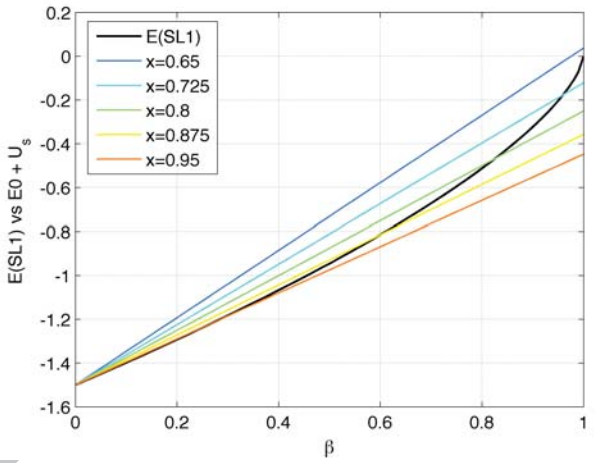

Figure 4: Intersection with $E(x_{SL_1}, \beta)$ and right side of Eq. (16) in correspondence of SL_1.

Another main difference with the traditional Δv is that, due to the constraint in the direction of the SRP acceleration, the spacecraft cannot be disposed toward the Sun by closing the curves at SL_1. In the case of traditional propulsion, the ΔE is defined as Olikara et al. (2013):

$$\Delta E = E_{L_2} - E = \frac{1}{2}(V_{clsr}^2 - V^2) < 0, \tag{18}$$

where, V_{clsr}^2 is introduced in Appendix Appendix A, Eq (A.2). The shape of the ZVC for closure is given by the energy of L_2. V_{clsr} can be computed at any

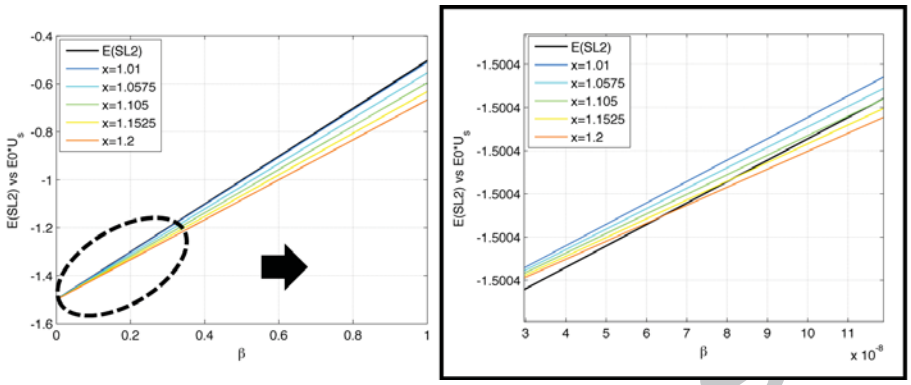

Figure 5: Intersection with $E(x_{SL_2}, \beta)$ and right side of Eq. (16) in correspondence of SL_2 with zoom in correspondence of region of intersection.

point where the motion is permitted with the only constraint of $V_{clsr}^2 > 0$ (no point inside the forbidden region). In case of SRP, there is less freedom in the selection of the point since $U_s > 0$ is the constraint in ΔE, Eq (13). Indeed, U_s is function of β that assumes values within 0 and 1. Thus, $U_s^{min}(\beta = 0) < U_s(\beta) < U_s^{max}(\beta = 1)$ (where $U_s^{min}(\beta = 0) = 0$), so $0 < U_s(\beta) < U_s^{max}(\beta = 1)$. This constraint obliges the spacecraft to be always at the right-hand side of the maximum coordinate of SL_2 that occurs when $\beta = 1$.

U_s is the potential of SRP forces which are constrained in direction. The higher is β, the more the region around the Sun and the Earth decreases since SL_1 and SL_3 collapse in the center of mass (circa the Sun) and SL_2 gets very close to the Earth, as shown in Figure 1. In Figure 7, a comparison with SRP and Δv manoeuvres for the closure of the ZVC is shown. A point along the LPO is selected for the EOL manoeuvre (black star) which is at the left-hand side of L_2. As one can see, when SRP is used the Lagrangian point moves such that after the closure the spacecraft is disposed on a graveyard orbit around the Sun, Figure 7a-7b, while with traditional Δv the disposal is towards the Sun Figure 7c-7d.

This can be verified also by looking at Eq. (17), which, in the case considered, is simplified as:

$$\begin{aligned}\frac{1}{2}V_{P_1}^2 = \; & \frac{1}{2}(x_{P_1}^2 + y_{P_1}^2 - x_{SL_j}^2) - \mu_{Sun}(1-\beta)\left[\frac{1}{r_{Sun-SL_j}} - \frac{1}{r_{Sun-P_1}}\right] \\ & -\mu_{Earth}\left[\frac{1}{r_{Earth-SL_j}} - \frac{1}{r_{Earth-P_1}}\right],\end{aligned} \tag{19}$$

when, $\beta_0 = 0$. In order to achieve the closure at SL_j, it is necessary to satisfy Eq. (19). The left side of Eq. (19) contains the squared velocity for a generic point P_1, which is a positive term. Therefore, in order to demonstrate that with SRP the closure towards the Sun is note permitted, we can study all the sign of Eq. (19) to ensure that its left-hand side is positive (that means $V_{P_1}^2 > 0$). In this paper, only the case in which P_1 is between the Earth and SL_2 region is shown (see Figure 6); however, it can be easily demonstrated that we would achieve the same results if P_1 is one of the gray points in Figure 6. For the case shown in Figure 6, the condition of $V_{P_1}^2 > 0$ can be guaranteed only if P_1 stays at the right side of the Lagrangian point at which we want to close the curve (for example SL_1). This can be easily demonstrate for $\beta = 1$ when the gravitational effect of the Sun is counteracted by the SRP: the squared of the velocity can be positive only if the point is at the right-hand side of the Libration point. This result can be extended for cases where β is less than 1 by studying the sign of each terms in Eq. (19) accordingly. In conclusion, to ensure that $V_{P_1}^2 > 0$, the key point is that P_1 should stay at the right side of SL_2. This condition is necessary, but not sufficient to find β that closes the zero-velocity curves since, as already shown, there are some cases where a solution does not exist, for instance when the β required is higher than 1, as shown in Figures 4-5. Finally, it is interesting to note that, when the velocity in P_1 is zero, P_1 is coincident to SL_j.

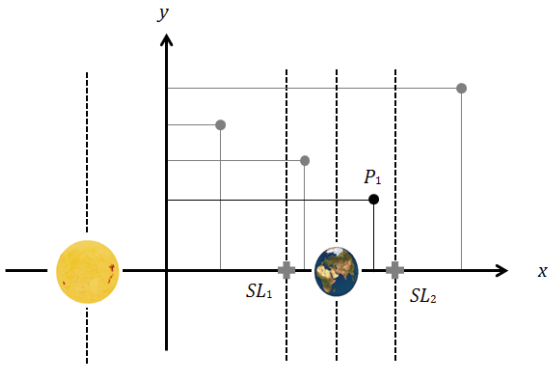

Figure 6: Reference system for studying the clousure in SL_j.

Table 2: Positions of L_1 and L_2 as a function of SRP.

β	x_{L_1}	x_{L_2}
0	0.989985982354727	1.010075200010617
1	$-0.105864912811615 \cdot 10^{-4}$	1.001739126300185

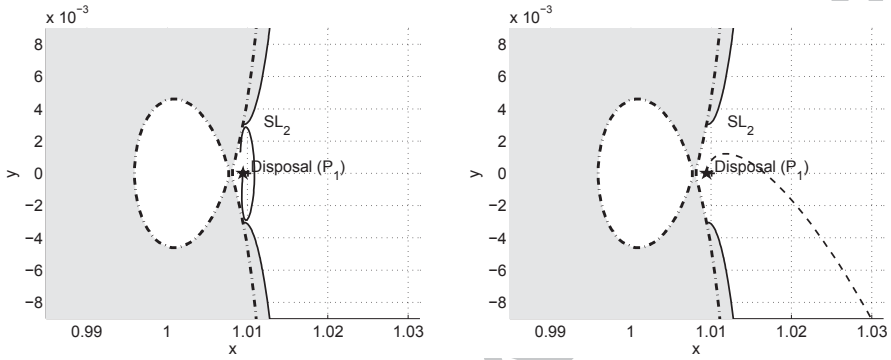

(a) EOL disposal with SRP. The β required is 0.02499.

(b) After the closure the spacecraft is at the right-hand side of SL_2.

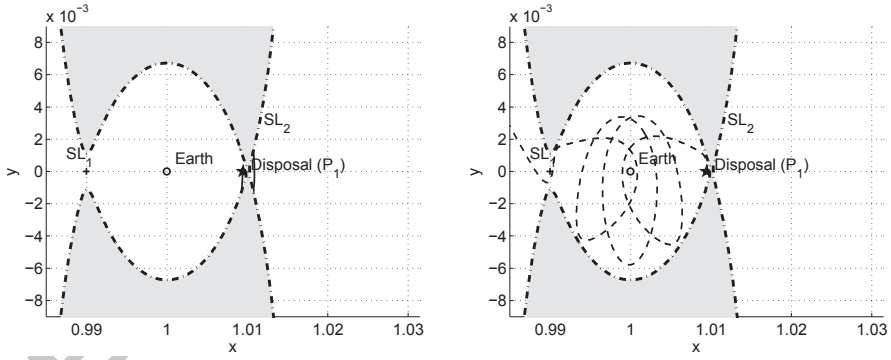

(c) EOL disposal with ΔV manoeuvre.

(d) After the closure the spacecraft is at the left-hand side of L_2.

Figure 7: Comparison of SRP and ΔV strategies when the point of disposal is at the left-hand side of the Lagrangian point L_2.

4.1. SRP equivalent Δv

The SRP equivalent Δv_{eq} quantifies how much theoretical Δv would be needed for a traditional propulsion system to augment the energy of the spacecraft to achieve the same energy level allowed by the use of a reflective SRP enhancing device. Note that, this Δv_{eq} cannot be effectively achieved by a propulsion system since the effect of SRP also changes the shape of the potential, which is not possible with a traditional propulsion-based approach. $E_0 = E(x_0, y_0, z_0, \dot{x}_0, \dot{y}_0, \dot{z}_0, \beta_0)$ (see Eq. (12)) is set as the initial energy of the system before the deployment and E_{SL_2} is set as the energy of the system after the deployment (Eq. (15) evaluated at SL_2). Now let's make the hypothesis that E_{SL_2} is achieved with a traditional propulsion system; therefore we can write the energy as in Eq. (15) by setting $\Delta\beta = 0$ and find V_{clsr} which is the velocity on the manifold after a hypothetical manoeuvre. From where the equivalent Δv_{eq} can be derived as:

$$\Delta v_{eq} = V_{clsr} - V = \sqrt{V^2 + 2\Delta\beta \frac{\mu_{Sun}}{r_{Sun-p}}} - V. \tag{20}$$

This equation will be applied in the next section in order to compare the proposed strategy with the one of Olikara et al. (2013) in term of Δv budget. The traditional Δv equation with the effect of SRP is reported in Appendix Appendix A in Eq. (A.2-A.3) derived by Olikara et al. (2013).

4.2. Disposal constraints

When disposing a spacecraft into a graveyard orbit around the Sun-(Earth+ Moon) system, it is important to identify safe regions in order to avoid the spacecraft from returning to the vicinity of the Earth, threatening its artificial satellites. This is especially true for spacecraft around L_1 (i.e., SOHO spacecraft), where a departing Δv is given towards L_2 in order to achieve the condition along the manifold to close the zero-velocity curves in SL_2 with SRP. This is done because it was demonstrated that the spacecraft cannot be bounded with this strategy in the region on the left of SL_1. For this reason, the deployment is done only beyond L_2 that means:

$$x > x_{L_2}. \tag{21}$$

In the case of a spacecraft at L_1, there are two more checks to take into account. One related, to the Earth's safe region: all trajectories that cross a

protected sphere around the Earth are discarded:

$$d_{Earth-p} \geq \frac{R}{AU} \tag{22}$$

where, AU is one astronomical unit, R was set equal to 60,000 km (greater than the GEO distance), $d_{Earth-p}$ is the distance Earth-Spacecraft,

$$d_{Earth-p} = ||\boldsymbol{r}_{Earth} - \boldsymbol{r}_p||, \tag{23}$$

and $\boldsymbol{r}_{Earth}$ and $\boldsymbol{r}_p$ are the distances of the Earth and the spacecraft from the center of mass. Secondly, among the trajectories that safely pass close to the Earth, some of them come back after few revolutions to L_1 towards the Sun; also in this case, the trajectories are discarded for the disposal and the condition in Eq. (21) holds.

5. Mission like scenarios

In this section, three ESA mission like scenarios are investigated: Gaia, Herschel and SOHO. The initial spacecraft parameters in terms of: initial deployable area (A_0), dry mass (m_{dry}), initial area-to-mass ratio (A_0/m_{dry}) and its correspondent lightness parameter (β_0) are shown in Table 3.

Gaia was recently placed in a Lissajous orbit around L_2 and its mission objective is to provide a 3D map of our galaxy (Hechler and Cobos, 2002). For the EOL analysis, several trajectories were selected starting along the Lissajous orbit, from 5.59 to 6.1 years since the start of the mission. Each unstable trajectory is obtained by integrating forward in time over 6 years. Figure 8a shows the area-to-mass requirement as a function of the curvilinear coordinate on the LPO (y-axis) and the time along the trajectory leg (x-axis). The time step selected along the trajectory leg is 0.05 in non-dimensional units, which, corresponds to 2.89 days. Figure 8b shows the magnitude of the Δv_{eq} due to the effect of the increasing energy of the system after the deployment. The spacecraft-Sun distance and the initial solar radiation pressure acceleration of Gaia are represented in Figure 9 as a function of the curvilinear coordinate on the Lissajous during six years of disposal. This also shows that the peaks in the area-to-mass ratio required are due to the fact that, along one trajectory, the spacecraft motion oscillates around the Hill's curves. Finally, it is interesting to compare the equivalent Δv_{eq}, Figure 8b with the traditional Δv (Olikara et al. (2013) and Colombo et al. (2014)) in

Figure 10. In the case of using a traditional propulsion system, the energy is decreased rather than increased by giving a Δv to close the curve as said in Section 4. For this traditional case it is not always possible to perform the manoeuvre close to the departing epoch from the initial orbit as the white area in Figure 10 is representative of the forbidden region; where, the manoeuvre can not be performed. This does not happen when exploiting SRP since the shape of the potential is changing and the velocity of the spacecraft does not change at the moment of the deployment.

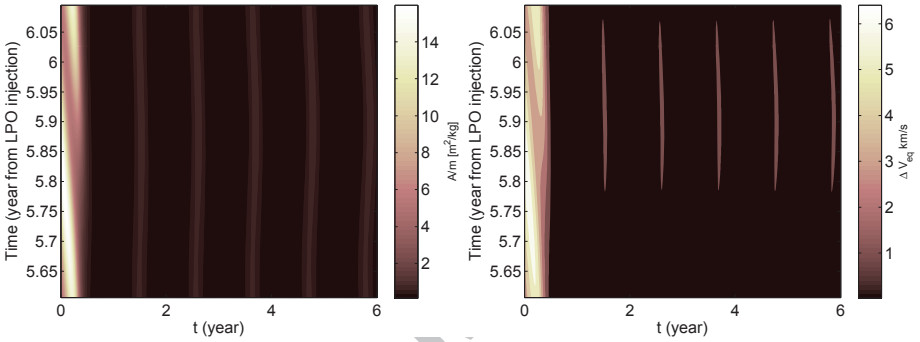

(a) Gaia area-to-mass ratio for disposal within six years.

(b) Gaia Δv_{eq} for the closure in SL_2 within six years.

Figure 8: Gaia area-to-mass ratio and equivalent Δv_{eq}, figure from Colombo et al. (2014).

Herschel was lunched in 2009 (Bauske, 2009) and its mission objective was to study the stars and galaxy formations. Herschel was placed in a halo orbit around L_2 with a period of 180 days. To study the disposal of Herschel in this work, 40 trajectories, equally distributed along the halo were selected. The time step along the halo was set to 4.6 days; where, the initial condition considered along the halo is on the side further from the Sun. Each single unstable trajectory is obtained by integrating forward in time for 6 years. The time step selected along the trajectory leg is 0.05 in non-dimension units, which corresponds to 2.89 days. Figure 11a represents the required area-to-mass ratio at the EOL. With respect to Gaia, the maximum area required is higher since Herschel has a higher total mass than Gaia. Consequently, the trend in the equivalent Δv_{eq} is also higher (see Figure 11b).

SOHO was lunched in 1995 and it was placed in a halo orbit with a period of 178 days around L_1, therefore the closure of the zero velocity curves in SL_2

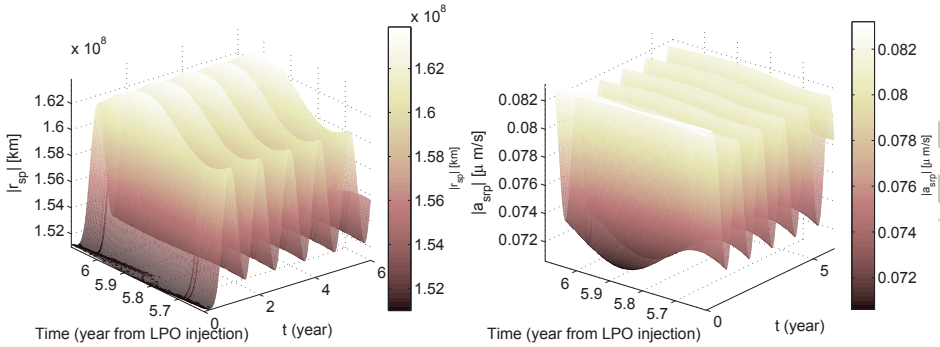

(a) Distance from the Sun. (b) SRP acceleration.

Figure 9: Distance from the Sun and SRP acceleration for Gaia $A/M_{dry} = 0.059$ m^2/kg.

should be done more carefully than in the case of Herschel and Gaia. After the injection from the halo to the unstable manifold towards the outer system, the disposal was investigated up to 6 years from the moment of injection. In the case of SOHO, it is necessary to carefully select the trajectories crossing the region of the Earth as outlined in Section 4.2. Figure 12a shows, as for Herschel and Gaia, the trend in the area-to-mass ratio required at the EOL. In terms of the results, SOHO is a satellite with a similar mass magnitude as Gaia. Since SOHO is placed in halo around L_1, it is interesting to note that the disposal is not always possible when compared with Herschel and Gaia cases. Indeed, it is possible to note that the white strips correspond to two class of trajectories: the one that goes bellow 60,000 km from Earth and the one that never passes by the gateway at L_2 (after several revolutions around the Earth, this trajectory goes back towards the Sun). Moreover, the coloured stripes shows when the spacecraft crosses the L_2 gateway; therefore, some unstable trajectories can spend several years crossing the Earth region and then reaching L_2, for example, after two years, which is not a fast and efficient disposal solution. The range of values in the area-to-mass ratio and in the Δv_{eq} for SOHO are an average of the Herschel and Gaia cases (see Figure 12). As already proved, when exploiting SRP it is not possible to dispose the spacecraft towards the Sun as for the Δv manoeuvre. However, Van Der Weg et al. in Colombo et al. (2014) presented a comparison in the Δv required for SOHO mission for a disposal towards the Sun and towards the outer part of the solar system, after L_2. It can be seen that the order of

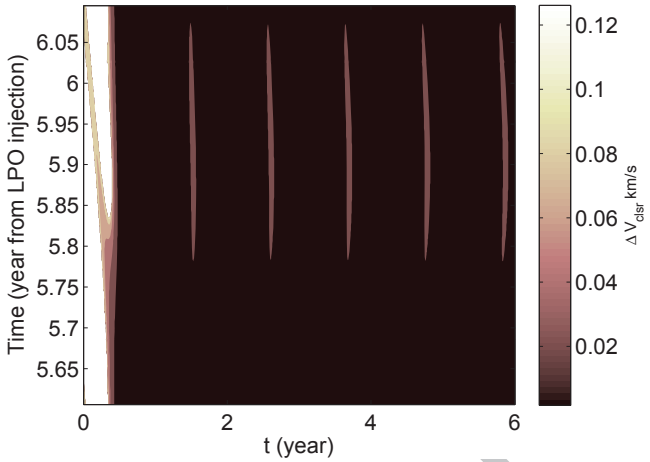

Figure 10: Gaia Δv for the closure in L_2 within six years with traditional propulsion, where the initial β_0 of Gaia is included in the dynamics.

magnitude in the required Δv is similar for both the disposal options. The main difference is in the additional operational cost of transferring from L_1 to L_2 that it is the only option when using SRP.

Table 3: Initial spacecraft parameters (Colombo et al., 2014).

S/C	A_0	m_{dry}	A_0/m_{dry}	β_0 (@A_0/m_{dry})
Gaia	69	1392	0.059	$8.98 \cdot 10^{-5}$
Herschel	16	3144	0.0051	$7.803 \cdot 10^{-6}$
SOHO	22	1602	0.021	$3.2 \cdot 10^{-5}$

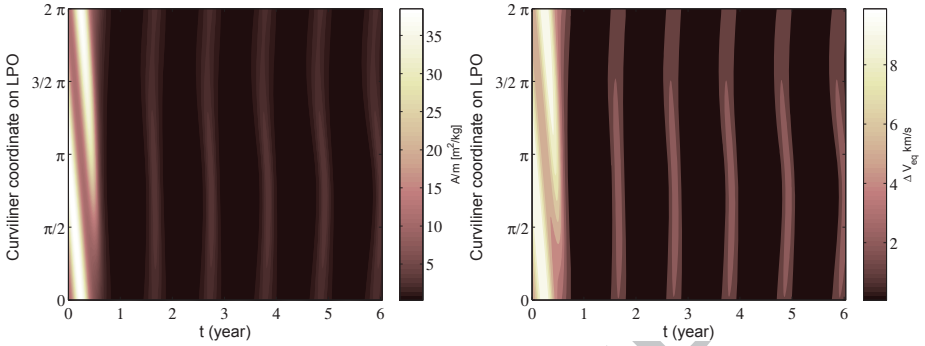

(a) Herschel area-to-mass ratio for disposal within six years.

(b) Herschel Δv_{eq} for the closure in SL_2 within six years.

Figure 11: Herschel area-to-mass ratio and equivalent Δv_{eq}.

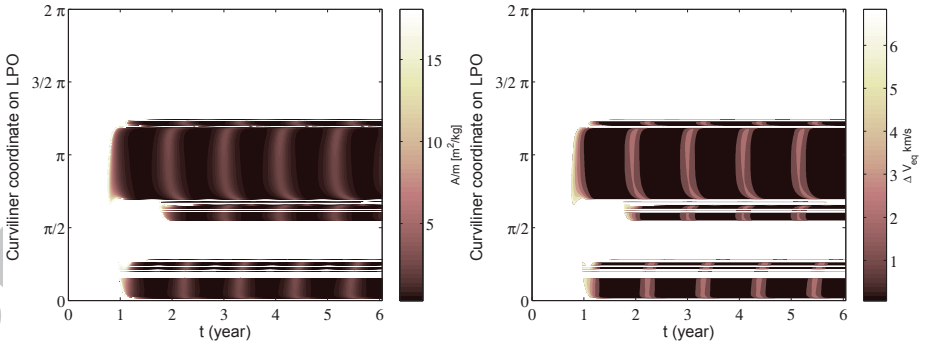

(a) SOHO area-to-mass ratio for disposal within six years.

(b) SOHO Δv_{eq} for the closure in SL_2 within six years.

Figure 12: SOHO area-to-mass ratio and equivalent Δv_{eq}.

5.1. Deployable Structure solutions

The minimum required delta area in the CR3BP-SRP is a deployed square area with a span of around 28 m for Herschel, an equivalent 21 m-span for SOHO and and 11 m-span for Gaia as shown in Table 4, where the range in the area-to-mass ratio presented in Figures 8a, 11a and 12a are also shown in the table. An additional EOL device for Herschel and Gaia missions cannot be easily achieved with additional flaps since their current sunshade configuration in term of shape does not allow the deployment of flaps. Instead, SOHO can potentially support additional solar panel flaps; however, the area provided by the solar panel is too small to support 20-m span area (i.e., solar concentrator). Note that JAXA has recently demonstrated the capability to deploy a 20 m-span sail with the Ikaros mission (Tsuda et al., 2013). Therefore, the disposal of Herschel seems to be the most technologically challenging to achieve with a deployed area due to the required 28 m span. However, spacecraft with the same characteristics in terms of configurations and masses such as Herschel, Gaia and SOHO, would require an specifically designed EOL stabilising deployable cone sail like the one used for attitude control (i.e., GOES mission (DRL-101-08, 1996)) or the pyramid sail proposed by Ceriotti et al. (2014) in order to achieve passive attitude stabilisation. In the cases studied, the EOL change in area is on the order of a 20 m-span square sail which will cover the spacecraft bus when deployed. Thus, a different configuration should be investigated to accommodate the area required (for example if the spacecraft's sunshade is covered by the EOL device, the EOL area should be bigger enough to include the shaded sunshade area). Importantly, this study shows that, the EOL phase should be taken into account as part of the mission design; in this way, it would be possible to include additional deployable areas which would expand on the existing projected area of the satellite; where, the final shape configuration should be such that it guarantees passive attitude stabilisation.

Table 4: Required reflective area and lightness parameter.

S/C	A/m [m^2/kg]	β(@A/m)	A_{min} [m^2]	ΔA_{min} [m^2] (m-span[8])
Gaia	0.135-15.98	$2.1 \cdot 10^{-4}$-0.02446	187.92	118.92 (10.9)
Herschel	0.266-38.52	$4.06 \cdot 10^{-4}$-0.059	836.304	820.304 (28.64)
SOHO	0.28-18.08	$4.35 \cdot 10^{-4}$-0.028	448.56	426.56 (20.65)

5.2. Discussion

The main features of the disposal strategy by means of solar radiation pressure for the zero velocity curves closure are that the device should be constrained to be sun-pointing, thus a self-stabilised deployable structure is required. The disposal using SRP can be achieved to close the zero velocity curves at SL_2 (the condition of closing the curves at SL_1 and dispose the spacecraft towards the Sun can not be achieved). It should be also taken into account that, to inject the spacecraft onto the unstable manifold a small Δv manoeuvre is required for the current spacecraft in a LPO. Since the acceleration of SRP is a function of the inverse square of the Sun-spacecraft distance, the minimum required area for the disposal is lower if the deployment is done far away from the Sun. Thus, SL_2 is much closer to L_2. Therefore, it is possible to better protect the L_2 region. Note that, half of the nominal halo orbit is also protected from spacecraft impact hazards once the curves are closed because it is at the far side of L_2 and SL_2 with respect to the Sun. In the case where the energy associated to the spacecraft initial orbit is higher, a higher area is required to perform the closure of the zero velocity curves at the same distance from the Sun as already proved for traditional propulsion by Olikara et al. (2013).

In order to verify the robustness of the SRP EOL strategy for LPO missions, we first focus on the effect of the Earth's orbit eccentricity on to the required area calculated using the CR3BP-SRP approximation as will be presented in Section 7. However, there are other aspects interesting to assess in future work such an analysis into the effects of uncertainties in the lightness parameter along with the SRP pointing direction. These uncertainties will affect the closure of the zero-velocity curves at SL_2. Thus, we expect that by including a margin in the area, after the deployment, the spacecraft reaches an energy greater than the one in SL_2, to compensate for these effects.

As previously stated, a Δv manoeuvre is required to leave the LPO. However, this depends onto the type of technology. For example, current missions to LPO use a traditional propulsion system throughout the normal mission lifetime. Therefore it is more convenient to use a small Δv manoeuvre to leave the LPO rather than SRP, this Δv can be achieved by using the attitude control engines. Conversely, for future solar sail missions to LPO, it would be interesting to exploit SRP also to leave the LPO. In this way,

[8] E.g., squared flap or additional EOL device.

two consecutive deployments are needed to fall off the LPO and to close the zero-velocity curves in SL_2.

6. Elliptic restricted-three body problem

Once the requirements for the closure of the zero-velocity curves have been defined in the CR3BP-SRP, it is of interest to verify how the effect of the Earth's orbit eccentricity affects the area needed for the closure. The dynamics of the Elliptic Restricted Three-Body Problem (ER3BP) for a sun-pointing (ER3BP-SRP) reflective surface are written in a non-dimensional, non-uniformly rotating and pulsating reference frame (Szebehely and Giacaglia, 1964; Baoyin and McInnes, 2006), where the motion of the Earth+Moon around the Sun is described by an ellipse:

$$r = \frac{a(1-e^2)}{(1+e\cos f)}. \tag{24}$$

In Eq. (24), a is the semimajor axis, f is the true anomaly and e is the eccentricity of the primaries (Earth+Moon barycentre with respect to the Sun) when their dynamics are described in the two-body problem. A coordinate system which rotates with the variable angular velocity $\dot{f}$ is introduced. The angular velocity is given by Kepler's third law as:

$$\frac{df}{dt} = \dot{f} = \frac{h}{r^2} = \frac{\tilde{\mu}^{\frac{1}{2}}(1+e\cos f)^{\frac{1}{2}}}{a^{\frac{3}{2}}(1-e^2)^{\frac{3}{2}}}, \tag{25}$$

where $\tilde{\mu}$ is $G \cdot (M_{Sun} + M_{Earth+Moon})$ and G is the constant of gravitation. Thus, the equation of motions for the non-dimensional synodic frame are (Szebehely and Giacaglia, 1964):

$$\begin{cases} x'' - 2y' = \omega_x \\ y'' + 2x' = \omega_y \\ z'' = \omega_z \end{cases} \tag{26}$$

where, ω is the potential function of the system and it is defined as:

$$\omega = \frac{\Omega}{1+e\cos f} \qquad\qquad \Omega = \Omega' - \frac{1}{2}(1+e\cos f)z^2 \tag{27}$$

with Ω' as:

$$\Omega' = \frac{1}{2}(x^2+y^2+z^2) + (1-\beta)\frac{\mu_{Sun}}{r_{Sun-p}} + \frac{\mu_{Earth}}{r_{Earth-p}}. \tag{28}$$

The symbol [$'$] denotes the derivation with respect to the true anomaly (i.e. pulsating coordinate). The definition of r_{Sun-p} and $r_{Earth-p}$ is the same as shown previously of Eq. (3) and Eq. (4) respectively. Moreover, the transformation that introduces dimensional coordinates ($\mathbf{r}_d$ and $\dot{\mathbf{r}}_d$) in the synodic frame from the non-dimensional pulsating coordinates ($\mathbf{r}$ and $\mathbf{r}'$) is given by

$$\begin{cases} \mathbf{r}_d = \mathbf{r} \cdot r \\ \dot{\mathbf{r}}_d = \mathbf{r}' \cdot r\dot{f} \end{cases} . \tag{29}$$

A similar approach that has been used for the CR3BP-SRP can be adopted to find the position of the pseudo Libration point for a sun-pointing reflective area in the ER3BP-SRP starting from Eq. (26). The five equilibrium points in the ER3BP-SRP have the same coordinates of the one in the CR3BP-SRP; thus, the equations in Table 1 holds for the ER3BP-SRP. The reason for the invariance in the Libration points in the synodical system is that in Eq. (26) it is possible to separate the variables as a function of the true anomaly from the other variables (Szebehely and Giacaglia, 1964). Figure 13 shows a trajectory for Gaia when departing at 195.2 [deg] of the Earth+Moon barycentre position and Eq. (26) is integrated over 15.5 years. From this figure it can be seen that there is a periodicity in the trajectory as the spacecraft return close to Earth every 15.5 years. The spacecraft's position when the Earth+Moon barycentre is at the pericenter or apocenter are also shown along the trajectory. Finally, the trajectory in the ER3BP (black line) is also compared with the one solved in the CR3BP approximation (dashed line).

The ephemeris of Gaia in a sidereal reference frame in dimensional coordinates (Alessi, 2015) was transformed to synodical non-dimensional coordinates in the osculating CR3BP (Goméz et al., 1991b). This full body transformation was compared to the one in the ER3BP. The two solutions were compared when the spacecraft performs one year of its orbit from 1/4/2019 to 1/4/2020 which is within the disposal window for Gaia.

6.1. Energy with the effect of the Earth's orbit eccentricity

Due to the non-autonomous nature of the ER3BP-SRP, the dynamics does not allow the use of the Jacobi integral. Thus, the energy in the ER3BP-SRP

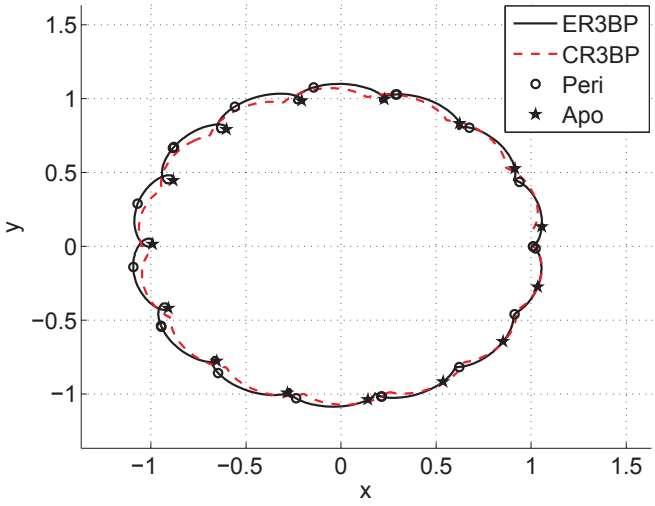

Figure 13: Comparison of Gaia's trajectory evolution in the ER3BP (black line) when leaving the orbit at 195.2 [deg] and in the CR3BP (dashed line). The propagating time is 15.5 years.

(Szenkovits et al., 2004; Campagnola et al., 2008) is a function of an integral, I:

$$E(f_0, \boldsymbol{x}(f_0), f, \beta_0) = \frac{1}{2}(x'^2 + y'^2 + z'^2) - \omega + I \tag{30}$$

where, ω is defined as in Eq. (27) and E is the energy in the ER3BP-SRP. The integral, I is defined as:

$$I = \int_{f_0}^{f} \frac{e \sin \tilde{f}}{(1 + e \cos \tilde{f})^2} \Omega' d\tilde{f}. \tag{31}$$

The integral I oscillates along the trajectory and it has a minimum and a maximum at the Earth+Moon pericenter and apocenter condition respectively. The left term in Eq. (30) excluding I is the relative energy of the system. The relative energy oscillates along the trajectory and its oscillations are such that when added to I the total relative energy E is constant. This happened because the state vector is a solution of Eq. (26); thus, a function of the true anomaly only. In the ER3BP, it is not possible to define a constant of motion, but having fixed the initial true anomaly of the system (f_0)

when leaving the LPO, the energy is conserved along a specific trajectory.

7. Energy approach and strategy description in the ER3BP-SRP

When taking into account of the effect of the Earth's eccentricity, a similar approach to the CR3BP-SRP is adopted. Eq. (16) still holds but Eq. (15) becomes:

$$E(\boldsymbol{x}, \beta_0, \Delta\beta) = \frac{1}{2}V^2 - \omega(\beta_0, \Delta\beta) + I(\beta_0, \Delta\beta), \tag{32}$$

for the ER3BP-SRP.

The main difference with the CR3BP is that in the ER3BP the representation of the Zero Velocity Curves (ZVC) is not unique and depends on the approximation of the integral I. The problem is that the integral cannot be solved; thus, depending on the approximation used for the integral, the ZVC seems to oscillate. This oscillation in the ZVC has already been highlighted by Campagnola et al. (2008); where, the approximation in the ZVC are not consistent with the dynamics of the system.

Thus, in this article the ZVC are not used as a tool to prove the closure at SL_2 since a unique and consistent representation of them does not exist. However, it is known that the energy of the Lagrangian points and the spacecraft are constant when f_0 is fixed (when leaving the LPO). For this reason the condition of closure in SL_2 in Eq. (16) still holds and it is verified for one re-entry trajectory of Gaia.

Note that, the effect of the Earth's eccentricity was investigated for the disposal of Gaia, since it requires a lower deployable area in the CR3BP-SRP. The aim is to determine how the eccentricity affects the proposed EOL disposal strategy.

8. Effect of the Earth's orbit eccentricity on the disposal strategy

The importance of considering the effect of the Earth's orbit eccentricity is clear when looking at Figure 14. The Figure 14 shows the dynamics of the spacecraft when leaving the LPO in correspondence of $f_0 = 195.2$ [deg] (Earth+Moon position around the Sun) in the ER3BP (black line) and in the CR3BP (dashed line). The simulation lasts for 30 years and while in the CR3BP the spacecraft doesn't re-enter in the ER3BP the spacecraft crosses the L_1-Earth-L_2 protected regions. This shows the importance of having an accurate dynamic representation of the spacecraft when performing the EOL disposal.

By using the condition in Eq. (16) where the energy is defined as in Eq. (32), it is possible to identify the required lightness parameter and area-to-mass ratio to increase the energy up to the energy of SL_2. The time along the trajectory where the deployment is performed is 6.9 years and the dynamics with the sun-pointing reflective structure deployed are then integrated for 600 years to verify the closure condition, Figure 15. The required lightness parameter is $2.561 \cdot 10^{-4}$ which corresponds to an area-to-mass ratio of 0.1674 [m^2/kg]. The Δ energy between the spacecraft and SL_2 (Figure 16) is also verified before and after the deployment. As shown in Figure 16, the spacecraft reaches the energy of the pseudo Libration point after the deployment.

By observing Figure 15 at the Earth's close approach, we can conclude that the energy condition $E = E_{SL_2}$ is reached even if we can not have a representation of the ZVC in the ER3BP.

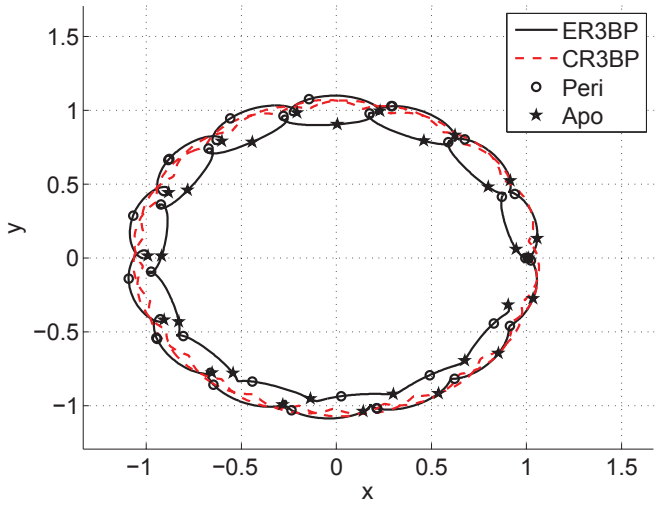

Figure 14: Trajectory evolution in the CR3BP (dashed line) and in the ER3BP when leaving the LPO at $f_0 = 195.2$ [deg]. The simulation time is of 30 years.

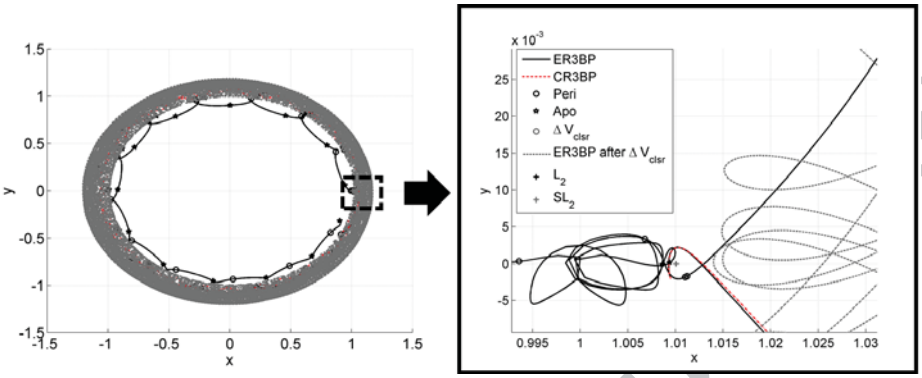

Figure 15: Trajectory evolution in the ER3BP (gray dashed line) after the deployment over 600 years of simulation time. The black line is the trajectory evolution in the ER3BP if within 30 years no deployment is performed. The dashed-dot line is the trajectory evolution in the CR3BP within 30 years of integration time.

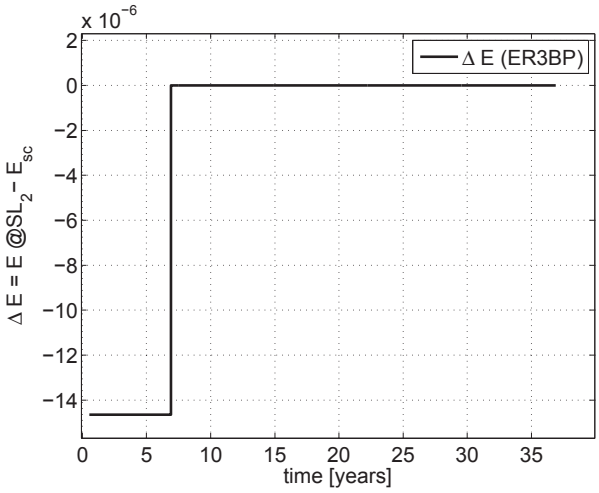

Figure 16: Δ energy between SL_2 and the spacecraft.

9. Conclusion

This paper proposes an end-of-life strategy which uses a solar radiation enhancing deployable device to close the zero velocity curves at the pseudo Lagrangian point SL_2, preventing the spacecraft's Earth return. The simulations have focused on studying the motion of the spacecraft after the deployment of a device at one location along the unstable manifold. The comparison of the unstable manifolds computed with and without the effect of SRP show that the positions along the manifolds are slightly shifted. Therefore, if the SRP is not taken into account after the injection its effect can add an uncertainty on when the deployments should be performed. This study was verified for three ESA missions: Herschel, Gaia and SOHO when SRP is included after the manifold injection. Those spacecraft are placed in a halo orbit, a Lissajous orbit around L_2 and in a halo orbit around L_1 respectively. It was demonstrated that, after the injection onto the unstable manifold, it is not always possible to close the Hill's curves. For example, for a spacecraft around L_1 such as SOHO, as for some trajectories the spacecraft passes too close to the Earth or after a few revolutions around the Earth, they return towards the Sun. A minimum area is required the further the spacecraft distant from the Sun. The minimum required change in area in the CRTBPs is around 28 m-span for Herschel, 21 m-span for SOHO and 11 m-span for Gaia.

Furthermore, an area margin should be included to counteract the effect of perturbations in the full body system. Therefore, a preliminary analysis was performed in the ER3BP-SRP (Szebehely and Giacaglia, 1964) to verify the effect of the Earth's orbit eccentricity on the disposal strategy and to possibly quantify the area margin that should be included. From this study, it appears that the effect of the Earth's orbit eccentricity can not be neglected when performing the closure of the zero-velocity curves. For the ER3BP, a representation in the ZVC is not possible. However, the energy approach formulated in the CR3BP can still be used. Further studies will include advanced SRP models that takes into account of the shape of the spacecraft and will analyse the ER3BP-SRP for more initial conditions.

Acknowledgement

C. Colombo and S. Soldini would like to acknowledge the ESA contract No. 4000107624/13/F/MOS under which this study was initiated and the

other members of the study team and ESA technical officers: E. M. Alessi, F. Letizia, M. Vasile. , M. Vetrisano, W. van der Weg, M. Landgraf and F. Renk. In particular, we thank E. M. Alessi for providing the initial orbit of Gaia in the inertial reference system. C. Colombo was supported by the FP7 Marie Curie grant 302270 (SpaceDebECM - Space Debris Evolution, Collision risk, and Mitigation).

Appendix A. Traditional Δv with the effect of solar radiation pressure

In this section, the strategy with the Δv disposal by Olikara et al. (2013) is presented here with the additional effect of the SRP perturbation. In case that Olikara et al. (2013) would have taken into account the effect of SRP, the condition of closure would be:

$$E_{SL_2} = \frac{1}{2}V_{clsr}^2 - \frac{1}{2}(x^2+y^2) - (1-\beta_0)\frac{\mu_{Sun}}{r_{Sun-p}} - \frac{\mu_{Earth}}{r_{Earth-p}} \tag{A.1}$$

and V_{clsr} is now defined as:

$$V_{clsr} = \sqrt{2E_{SL_2} + (x^2+y^2) + 2\left[(1-\beta_0)\frac{\mu_{Sun}}{r_{Sun-p}} + \frac{\mu_{Earth}}{r_{Earth-p}}\right]}. \tag{A.2}$$

The Δv for closing the zero-velocity curves when an initial effect of SRP (β_0) is included is:

$$\Delta v_s = V_{clsr} - V, \tag{A.3}$$

as shown in Figure 10.

Now, if Eq. (A.2-A.3) is compared with the one presented by Olikara et al. (2013) it is possible to verify that the effect of SRP implies a higher Δv. Indeed, with the same initial state vector V, the Δv_s required (when SRP is considered) would be higher than the Δv required without considering SRP. In conclusion, also when using traditional Δv to close the curves, it can be useful to include a margin in the Δv due to the uncertainty in the reflectivity of the spacecraft since SRP is one of the major perturbations after the gravitational effect. Thus the solution presented in Figure 10 is slightly different when compared with the results of Olikara et al. (2013), for instance, the location of the forbidden region is shifted.

References

Alessi, E. M. (2015), 'The reentry to earth as a valuable option at the end-of-life of libration point orbit missions', *Advances in Space Research* **55**(12), 2914–2930.

Baoyin, H. and McInnes, C. R. (2006), 'Solar sail equilibria in the elliptical restricted three-body problem', *Journal of Guidance, Control and Dynamics* **29**(3), 538–543.

Bauske, R. (2009), 'Operational manoeuvre optimization for the ESA missions Herschel and Planck', *Proceedings of the 21st International Symposium on Space Flight Dynamics, http://issfd.org/* .

Campagnola, S., Martin, L. and Newton, P. (2008), 'Subregions of motion and elliptic halo orbits in the elliptic restricted three-body problem', *Proceeding of AAS/AIAA Space Flight Mechanics Meeting, AAS 08-200, February, 2008* **130**, 1541–1556.

Ceriotti, M., Harkness, P. and McRobb, M. (2014), 'Variable-geometry solar sailing: the possibility of the quasi-rhombic pyramid', *Advances in Solar Sailing* pp. 899–919.

Colombo, C., Alessi, E. A., Van der Weg, W., Soldini, S., Letizia, F., Vetrisano, M., Vasile, M., Rossi, A. and Landgraf, M. (2015), 'End-of-life disposal concepts for libration point orbit and highly elliptical orbit missions', *Acta Astronautica* **110**, 298–312.

Colombo, C., Letizia, F., Soldini, S., Alessi, E. A., Rossi, A., Vasile, M., Vetrisano, M., Van der Weg, W. and Landgraf, M. (2014), 'End-of-life disposal concepts for libration point and highly elliptical orbit missions', *Final Report, ESA/ESOC contract No. 4000107624/13/F/MOS* .

DRL-101-08 (1996), *GOES I-M DataBook*, Contract NAS5-29500.

Elipe, A. (1992), 'On the restricted three-body problem with generalized forces', *Astrophysics and space science* **188**, 257–269.

Farrés, A. and Jorba, A. (2010), 'Dynamics of a solar sail near a halo orbit', *Acta Astronautica* **67**, 979–990.

Goméz, G., Jorba, A., Masdemont, J. and Simó, C. (1991a), *Dynamics and mission design near libration points: advanced methods for collinear points v. 3*, World Scientific Publishing Co. Pte. Ltd., Singapore.

Goméz, G., Jorba, A., Masdemont, J., Simó, C. and Rodriguez-Canabal, J. (1991b), 'Study refinement of semi-analytical halo orbit theory', *Final Report, ESA/ESOC contract No. 8625/89/D/MD(SC)* .

Hechler, M. and Cobos, J. (2002), 'Herschel, Planck and Gaia orbit design', *Proceedings of the 7th International Conference on Libration Point Orbits and Application, Parador d'Aiguablava, Girona, Spain, 10-14 June 2002* pp. 115–135.

Hyeraci, N. and Topputo, F. (2013), 'The role of true anomaly in balistic capture', *Celest Mech Dyn Astr* **116**, 175–193.

Koon, W. S., Lo, M. W., Marsden, J. E. and Ross, S. D. (2008), *Dynamical systems, the three-body problem and space mission design*, Marsden Books, ISBN 978-0-615-24095-4, California.

McInnes, A. I. S. (2000), Strategies for solar sail mission design in the circular restricted three-body problem, Master thesis, Purdue University.

McInnes, C. R. (1998), *Solar sailing: technology, dynamics and mission applications*, Springer, Glasgow, Scotland.

Olikara, Z., Goméz, G. and Masdemont, J. J. (2013), 'End-of-life disposal of libration point orbit spacecraft', *Proceedings of the 64th International Astronautical Congress, IAC-13.C1.82, Beijing, China, 23-27 September, 2013, CD-ROM* .

Olive, J. P., Overbeek, T. V. and Fleck, B. (2013), 'Soho monthly trending report', *SOHO/PRG/TR/769 Oct 15* .

Szebehely, V. (1967), *Theory of orbits in the restricted problem of three bodies*, Academic Press Inc., New York.

Szebehely, V. and Giacaglia, G. E. O. (1964), 'On the elliptic restricted three body problem', *The Astronomical Journal* **69**(3), 230–235.

Szenkovits, F., Makó, Z. and Csillik, I. (2004), 'Polynomial representation of the zero velocity surfaces in the spatial elliptic restricted three-body problem', *Pure Mathematics and Application* **15**(2-3), 323–322.

Tsuda, Y., Mori, O., Funase, R., Sawada, H., Yamamoto, T., Saiki, T., Endo, T., Yonekura, K., Hoshino, H. and Kawaguchi, J. (2013), 'Achievement of IKAROS Japanese deep space solar sail demonstration mission', *Acta Astronautica* **82**(2), 183–188.